Supplemental information

A highly simple and controllable nitrogen-doping method for carbon-based surface-enhanced Raman spectroscopy substrates

Machiko Marumi,[a] Xuke Tang,[a] V. Kesava Rao,[ab] Abdullah N. Alodhayb,[c] Manish M. Kulkarni,[d] Prabhat K. Dwivedi,[d] Fabio Lisi,[a] Yasutaka Kitahama,*[ab] Ting-Hui Xiao [aef] and Keisuke Goda *[abghi]

[a] *Department of Chemistry, The University of Tokyo, Tokyo 113-0033, Japan. Email: kitahama@g.ecc.u-tokyo.ac.jp, goda@chem.s.u-tokyo.ac.jp*
[b] *LucasLand, Tokyo 101-0052, Japan*
[c] *Department of Physics and Astronomy, College of Science, King Saud University, Riyadh, 11451, Saudi Arabia*
[d] *Centre for Nanosciences, Indian Institute of Technology Kanpur, Kanpur 208016, India*
[e] *Henan Key Laboratory of Diamond Optoelectronic Materials and Devices, School of Physics and Microelectronics, Zhengzhou University, Zhengzhou 450052, China*
[f] *Institute of Quantum Materials and Physics, Henan Academy of Sciences, Zhengzhou 450046, China*
[g] *Institute for Quantum Life Science, National Institute for Quantum and Radiological Science and Technology, Chiba 263-8555, Japan*
[h] *Institute of Technological Sciences, Wuhan University, Hubei 430072, China*
[i] *Department of Bioengineering, University of California, Los Angeles, California 90095, USA*

SEM images of the PAN-based SERS substrates

PAN-based substrates with unfused fiber morphology were obtained when the spin coating step was performed at 4000 rpm instead of 2700 rpm. This increased speed drastically reduced the amount of DMSO on the Si wafer, making the PAN nanomesh difficult to attach and not fusing during the subsequent carbonization step. SEM images of the unfused substrates are shown in Fig. S1. As shown in Fig. S2, the variation in wettability of the PAN-based fused substrate carbonized at 1200 ºC was compared with the non-fused substrate. The diameters of fused fibers in PAN-based substrates were measured using Digimizer image analysis software and are plotted in Fig. S3.
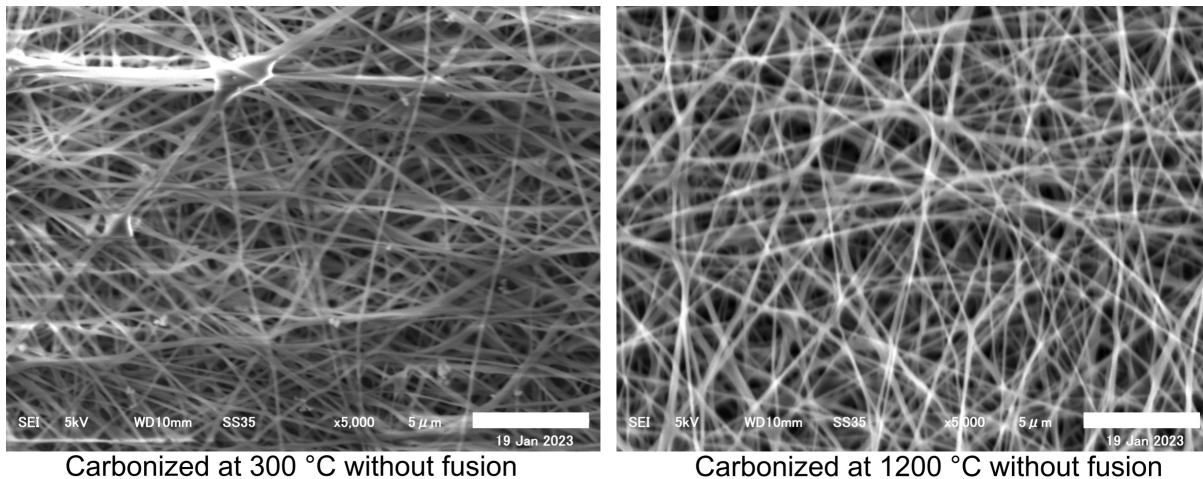
Carbonized at 300 °C without fusion   Carbonized at 1200 °C without fusion

Fig. S1 SEM images of unfused PAN-based SERS substrates, collected when the electrospun PAN nanomesh did not contain a sufficient amount of DMSO. The PAN-based substrates were carbonized at 300 ºC and 1200 ºC. Scale bars are 5 µm.

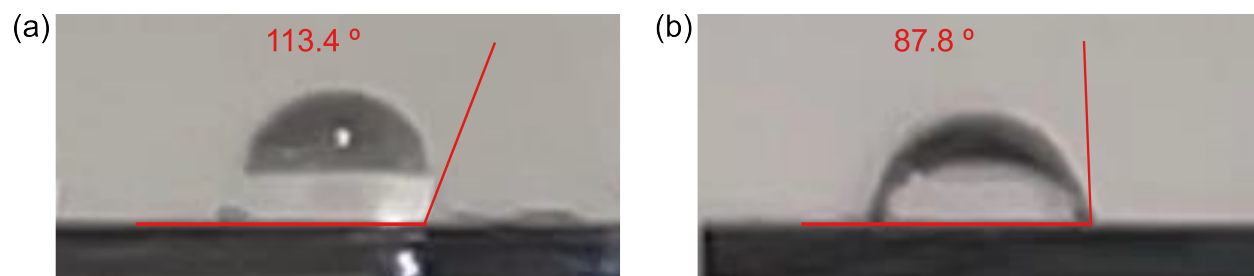(a) 113.4 º   (b) 87.8 º

Fig. S2 Pictures of water drop on the PAN-based substrates carbonized at 1200 ºC (a) with and (b) without fusion. The contact angles of the PAN-based SERS substrate carbonized at 1200 ºC with and without fusion were measured at 5 s after dropping and calculated by the half-angle method.
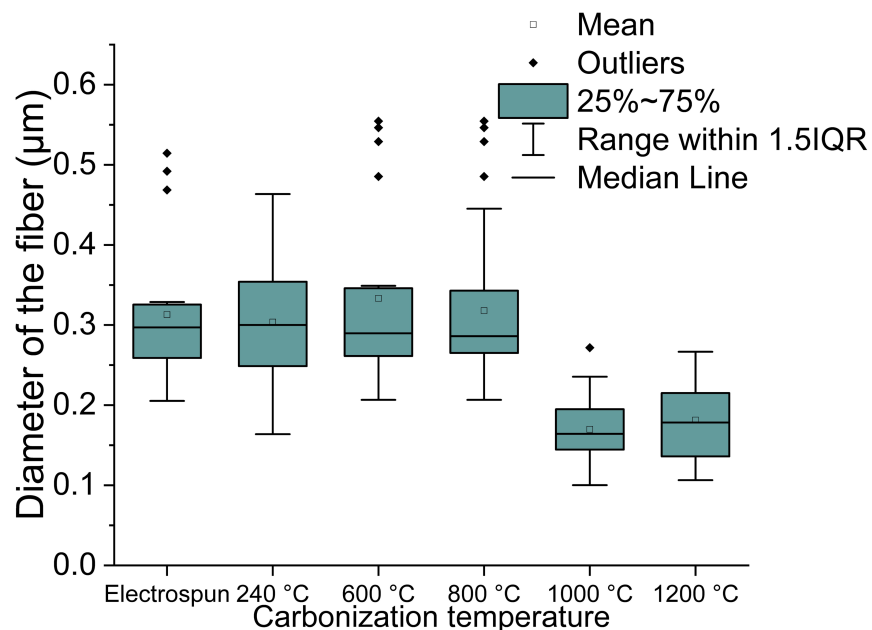
Fig. S3 Diameters of the fused PAN-based nanofibers. Box plot of diameters of the nanofibers (n ≥ 20) in the PAN-based SERS substrates carbonized at 240–1200 °C, derived from the SEM images.

EDS analysis of the PAN-based SERS substrates

To evaluate the chemical compositions of the PAN-based SERS substrates, they were examined by energy dispersive X-ray spectroscopy (EDS). shows the elemental compositions of the PAN-based SERS substrates as determined by EDS. The focus of this investigation is on the sulfur content and the nitrogen-to-carbon ratio of the prepared samples. Interestingly, while some flameproofed substrates manifested a sulfur content of 1%—above the detectable threshold of EDS—in others the sulfur was undetectable, probably because it was below the 1% threshold. This inconsistency suggests the persistent presence of the solvent used during the electrospinning post-flameproofing, which subsequently dissipates during the carbonization process, thereby eliminating the impact of sulfur doping on the SERS effect. Because the penetration depth of the X-ray radiation is several micrometers, the oxygen content included not only the PAN-based SERS substrates but also the SiO_2 layer on the silicon support, rendering an accurate oxygen ratio analysis difficult. Thus, the correlation between carbon and nitrogen ratios was also investigated. As the carbonization temperature increased, the nitrogen-to-carbon ratio decreased until reaching a value of 0.05 at a carbonization temperature of 1200 °C. Considering that the primary gases liberated from intermolecular reactions are HCN and N_2, the striking decrease in the nitrogen-to-carbon ratio observed in the substrate carbonized at 1200 °C is indicative of the progress of these intermolecular reactions.
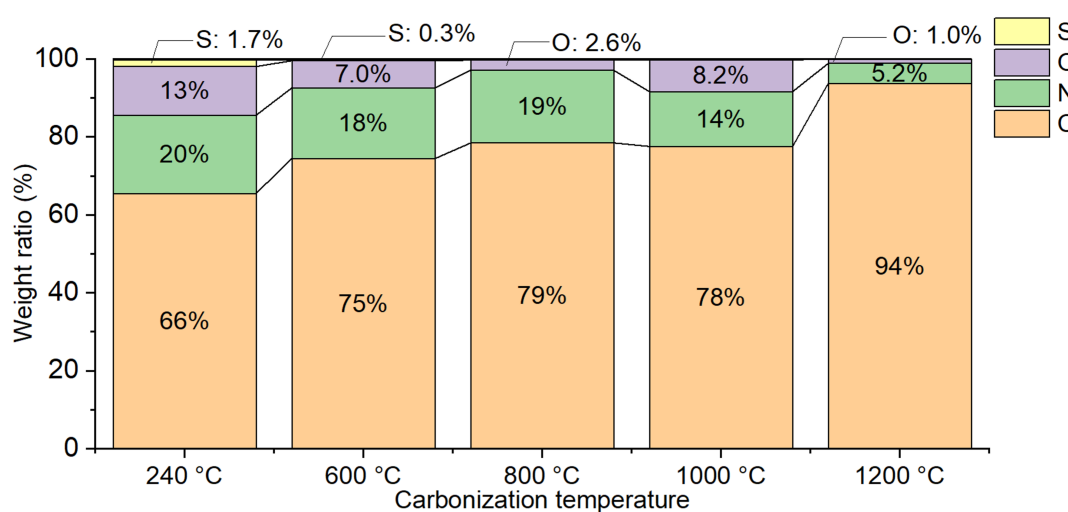
Fig. S4 Chemical compositions of the PAN-based SERS substrates. Weight ratios of elements in the PAN-based SERS substrates carbonized at 240–1200 ºC derived from the EDS measurements.

Raman spectra of the PAN-based SERS substrates

To evaluate defects in the PAN-based substrate, we subjected them to spontaneous Raman spectroscopy (Fig. S5(a)). This method exhibits exceptional sensitivity to sp2 bonding within the top 10 nm of the surface, due to substantial cross-sections facilitated by a dual resonance mechanism involving the Dirac cones inherent in graphene-like structures.[1] Raman spectral features within the carbon structure include the D-band at 1350–1370 cm^{-1} and the D'-band at 1620 cm^{-1}, both indicative of structural disorder and defects. In addition, the G band at 1580 cm^{-1} results from the in-plane motion of graphite.[2-5] When defects are present in the graphite structure, the D and D' bands appear in addition to the G band. The relative intensity of these bands to the G-band, referred to as the R-value (= $I_{D\text{-band}} / I_{G\text{-band}}$), increases with a higher incidence of defects, resulting in a broader band shape. On the other hand, the full width at half maximum (FWHM) of the G-band is a commonly used metric to measure the degree of graphitization. In highly oriented pyrolytic graphite (HOPG) and pristine graphene, the R-value and FWHM of the G-band are theoretically determined to be 0 and 14 cm^{-1}, respectively.[6] The spectral fitting was performed under the assumption that the peaks have a Gaussian shape. As shown in Fig. S5(b) and S5(c), the R values of the PAN-based substrate and the FWHM of the G band under 532 nm excitation showed a negative correlation with the carbonization temperature. Nevertheless, it is noteworthy that both the R-value and the FWHM of the G-band were significantly different from those observed for highly oriented pyrolytic graphite (HOPG), suggesting that the PAN-based substrates can be described as polycyclic aromatic compounds rather than polycrystalline graphite. Interestingly, despite having numerous structural defects compared to graphite, these PAN-based substrates still exhibited a pronounced SERS effect.
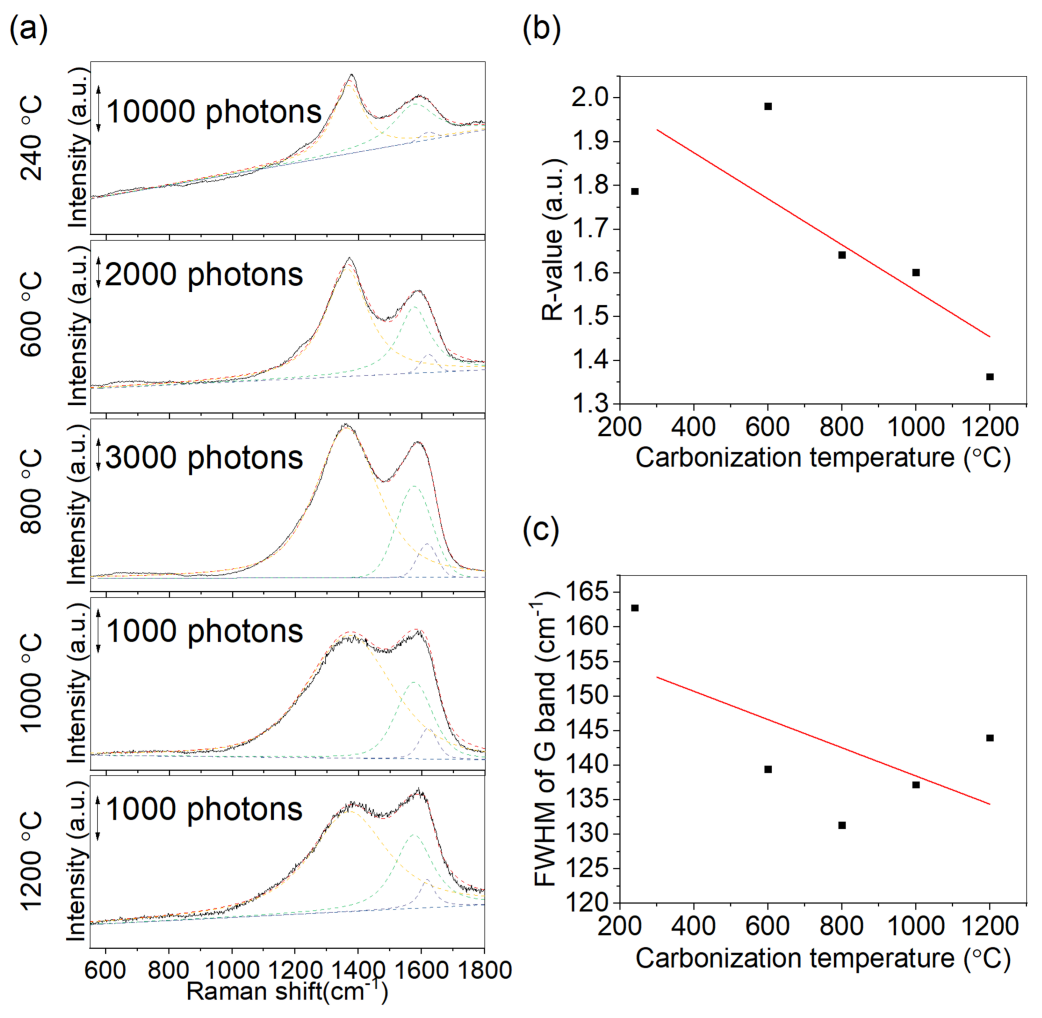
Fig. S5 Defects in the PAN-based SERS substrates. (a) Raman spectra of the PAN-based SERS substrates carbonized at 240–1200 ºC. (b) R-values (= $I_{\text{D-band}}$ / $I_{\text{G-band}}$) and (c) FWHM of G-band of the PAN-based SERS substrates carbonized at 240–1200 ºC.

XPS measurements of the PAN-based SERS substrates

Table S1 displays the precise assignments for X-ray photoelectron spectroscopy (XPS) spectra of the PAN-based SERS substrates. The elongated tails, observed on the higher energy side of both C1s and N1s peaks, suggest the existence of conjugated unsaturated bonds within the polymer.[7] Carboxyl groups are attributed to the O1s peaks, considered as by-products of cyclization reactions (Fig. S6).[8] These carbonyl groups are mostly on the surface of the substrate, which is exposed to the atmosphere. Because XPS is sensitive to the surface composition of a material, this explains why the proportion of oxygen content in the XPS results is higher than in the EDS characterization, while the agreement in the C and N content is very similar.

Table S1 Composition analysis and fitting parameters for the peaks in the XPS spectra of the PAN-based SERS substrates carbonized at 240–1200 ºC (see Fig. 3(a)).

|		Carbonization temperature	240 ºC	600 ºC	800 ºC	1000 ºC	1200 ºC	Attributed to
C1s	Peak1	B.E. (eV)	283.72	284.17	284.13	284.40	284.37	C-C
		Area (count/s)	2942	3302	3780	4066	4824	
		Percentage (%)	59.83	68.12	71.66	67.76	74.55	
	Peak2	B.E. (eV)	285.71	285.95	285.67	285.67	285.71	C with N
		Area (count/s)	1631	1213	1054	1147	1054	
		Percentage (%)	33.17	25.03	19.98	19.11	16.29	
	Peak3	B.E. (eV)	287.84	287.88	287.59	287.12	287.46	Satellite peak
		Area (count/s)	344	332	441	788	593	
		Percentage (%)	7.00	6.85	8.36	13.13	9.16	
N1s	Peak1	B.E. (eV)	397.70	397.98	397.68	397.95	398.38	Pyridinic-type structure, Conjugated imine
		Area (count/s)	739	757	761	354	134	
		Percentage (%)	43.88	52.61	52.63	39.25	27.35	
	Peak2	B.E. (eV)	399.12	399.62	399.85	499.51	400.66	Pyrrolic, Pyridon-N
		Area (count/s)	945	682	685	364	229	
		Percentage (%)	56.12	47.39	47.37	40.35	46.73	
	Peak3	B.E. (eV)				401.31	401.72	Graphitic N
		Area (count/s)				184.00	127.00	
		Percentage (%)				20.40	25.92	
O1s	Peak1	B.E. (eV)	530.37	530.19				C-OH, C=O
		Area (count/s)	1445.00	256.00				
		Percentage (%)	19.53	3.56				
	Peak2	B.E. (eV)	531.72	532.11	532.17	532.55	532.60	Pyridon-N
		Area (count/s)	5953	6943	8475	8282	8460	
		Percentage (%)	80.47	96.44	100.00	100.00	100.00	
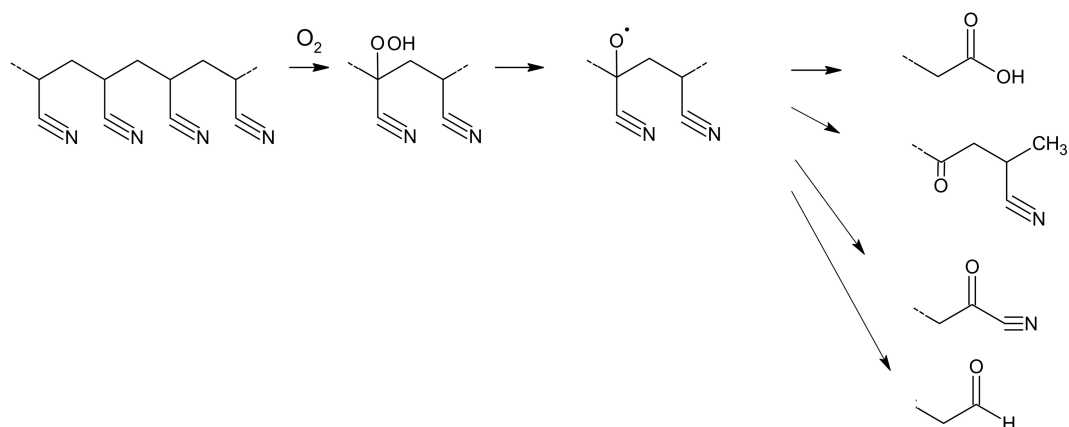
Fig S6 Main side reaction in the cyclization of PAN yielding carboxyl groups. In the pyrolysis of PAN, the first step is the cyclization reaction shown in Fig. 1 of the main text. However, several side reactions occur during the pyrolysis. In the investigated system, as revealed by IR spectroscopy, the primary side reaction is the formation of a carbonyl, leading to the appearance of the O1s peaks in the XPS spectrum. This reaction causes the scission of the polymeric chain, eventually resulting in the decrease of the conjugated system.

XRD measurements of the PAN-based SERS substrates

X-ray diffraction analysis (XRD, MiniFlex300/600) was applied to investigate the crystallographic properties of the PAN-based SERS substrates (Fig. S7). The peak fitting was conducted with SmartLab Studio Ⅱ. The (10) peak near $2\theta =16^{o}$ observed in the substrates carbonized at 240–600 °C, which is attributed to the hexagonal lattice and indicates the presence of C≡N groups, was completely obscured in the substrates carbonized at >800°C. In contrast, the (200) peak became sharper and stronger with increasing carbonization temperature, indicating that the ladder-like polymeric structure changed into a two-dimensional graphite-like structure through intermolecular reactions, and the new (10) peak near $2\theta = 43^{o}$ appeared, associated with carbon atoms in the same plane.[9] The distance of aromatic rings in the turbostratic layer (d_{200}) and the crystallite thickness (Lc) were calculated using Bragg's law (Equation 1) and Deby-Scherrer's equation (Equation 2), respectively (Table S2).[10,11]

$$d_{200}(\text{nm}) = \frac{\lambda}{2 \sin \theta_{002}} \qquad (1)$$

$$L_c(\text{nm}) = \frac{K\lambda}{\beta \cos \theta_{002}} \qquad (2)$$

where K is the Scherrer parameter, which is commonly taken as 0.94 for (002) diffraction trace.[12] λ is the wavelength of the X-ray source from Cu (0.154 nm). β and θ_{200} represent FWHM of the (002) peak and the diffraction angle attributed to the diffraction trace of (002) plane, respectively.
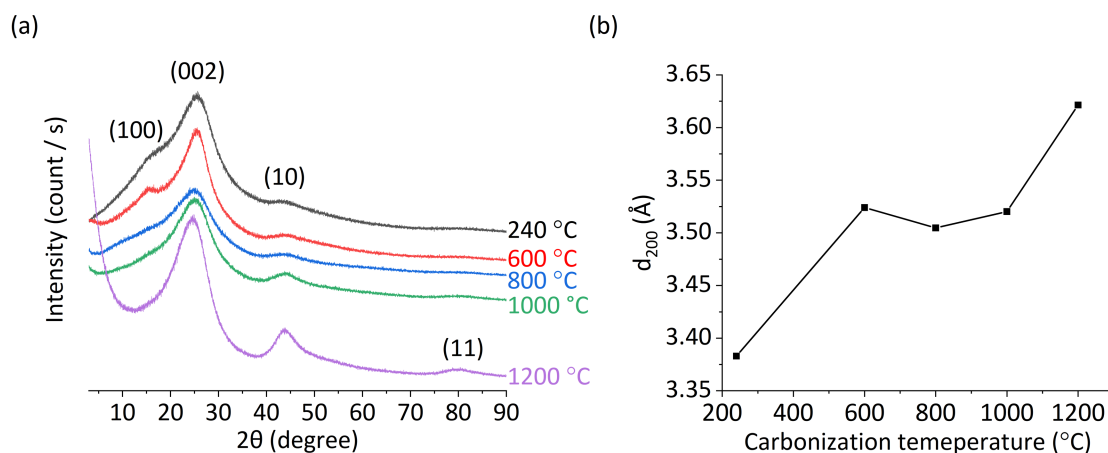
Fig. S7 Crystallinity of the PAN-based SERS substrates. (a) XRD spectra of the PAN-based SERS substrates carbonized at 240–1200 ℃. (b) Calculated d_{002} values of the PAN-based SERS substrates carbonized at 240–1200 ℃.

Table S2 Specifications of the PAN-based SERS substrates.

Carbonization temperature	240 ℃	600 ℃	800 ℃	1000 ℃	1200 ℃
$2\theta_{002}$ (°)	26.32	25.25	25.39	25.27	24.56
d_{002} (Å)	3.382	3.522	3.504	3.520	3.621
β (°)	12.95	6.92	12.54	10.10	7.99
Lc (Å)	6.576	12.28	6.779	8.419	10.62
Number of graphene layer (Lc/d_{002})	1.94	3.48	1.93	2.39	2.93

SERS performance of PAN-based substrates compared to other carbon-based substrates

To evaluate the SERS performance of PAN-based substrates, we compared them to commercial graphite-based substrates (Table S3) and other N-doped carbon-based substrates (Table S4). The EFs of the PAN-based substrate carbonized at 1200 °C and graphite substrates were computed using a 1 µM analyte solution (R6G and CV) under excitation at 532 nm. The analyte crystal powder served as a reference for EF computation. To assess the EF, we utilized the following formula:

$$EF = (I_{SERS} / I_{bulk}) \times (N_{bulk} / N_{SERS}) \tag{S1}$$

$$I_{SERS} = SERS\ peak\ intensity / (Laser\ power \times Exposure\ time) \tag{S2}$$

$$I_{bulk} = Raman\ peak\ intensity / (Laser\ power \times Exposure\ time) \tag{S3}$$

Here, I_{SERS} and I_{bulk} represent the peak intensity of SERS and spontaneous Raman signals, respectively. These intensities are normalized by dividing them by the excitation laser power and exposure time. N_{bulk} and N_{SERS} represent the number of analyte molecules probed in the bulk sample

through spontaneous Raman spectroscopy and in the aqueous solution spread on the substrate for SERS measurements, respectively, and can be expressed as follows:

N_{bulk} = (N_A × ρ × V) / *Molecular weight* = 7.14×10^{10} (R6G), 7.92×10^{10} (CV) (S4)

N_{SERS} = (N_A × *Concentration* × *Volume of the sample*) × (*Laser spot area* / *Substrate area*) (S5)

Here, N_A represents Avogadro's constant, and ρ is the density of the analyte crystal (1.28 g cm^{-3} for R6G and 1.19 g cm^{-3} for CV). The focal volume V and the laser spot area can be estimated using the following formula:[13]

$$\text{Laser spot diameter: } W_0 \text{ (m)} = \frac{1.22\lambda}{NA} = \frac{1.22 \times 5.32 \times 10^{-7}}{0.55} = 1.18 \times 10^{-6} \quad \text{(S5)}$$

$$\text{Focal depth: } Z_0 \text{ (m)} = \left(\frac{2\pi}{\lambda}\right) W_0^2 = \frac{2 \times 3.14}{5.32 \times 10^{-7}} \times (1.18 \times 10^{-6})^2 = 1.64 \times 10^{-5} \quad \text{(S6)}$$

$$\text{Focal volume: } V \text{ (m}^3\text{)} = \left(\frac{\pi}{2}\right)^{1.5} W_0^2 Z_0 = 4.51 \times 10^{-17} \quad \text{(S7)}$$

Here, λ represents the wavelength of the laser light (5.32×10^{-7} m), and NA is the numerical aperture (0.55). For the SERS measurements, we applied a sample volume of 2×10^{-6} L onto an area of 5×10^{-6} m^2.

Table S3 EF and limit of detection (LOD) for R6G and CV on the PAN-based substrate carbonized at 1200 °C and the graphite substrate.

Analyte	R6G		CV	
	EF	LOD	EF	LOD
PAN-based substrate	6.8×10^3	100 nM	3.2×10^3	700 nM
Graphite substrate	2.3×10^2	400 nM	8.4×10^1	1 μM

Table S4 Conventional N-doped carbon-based SERS substrates

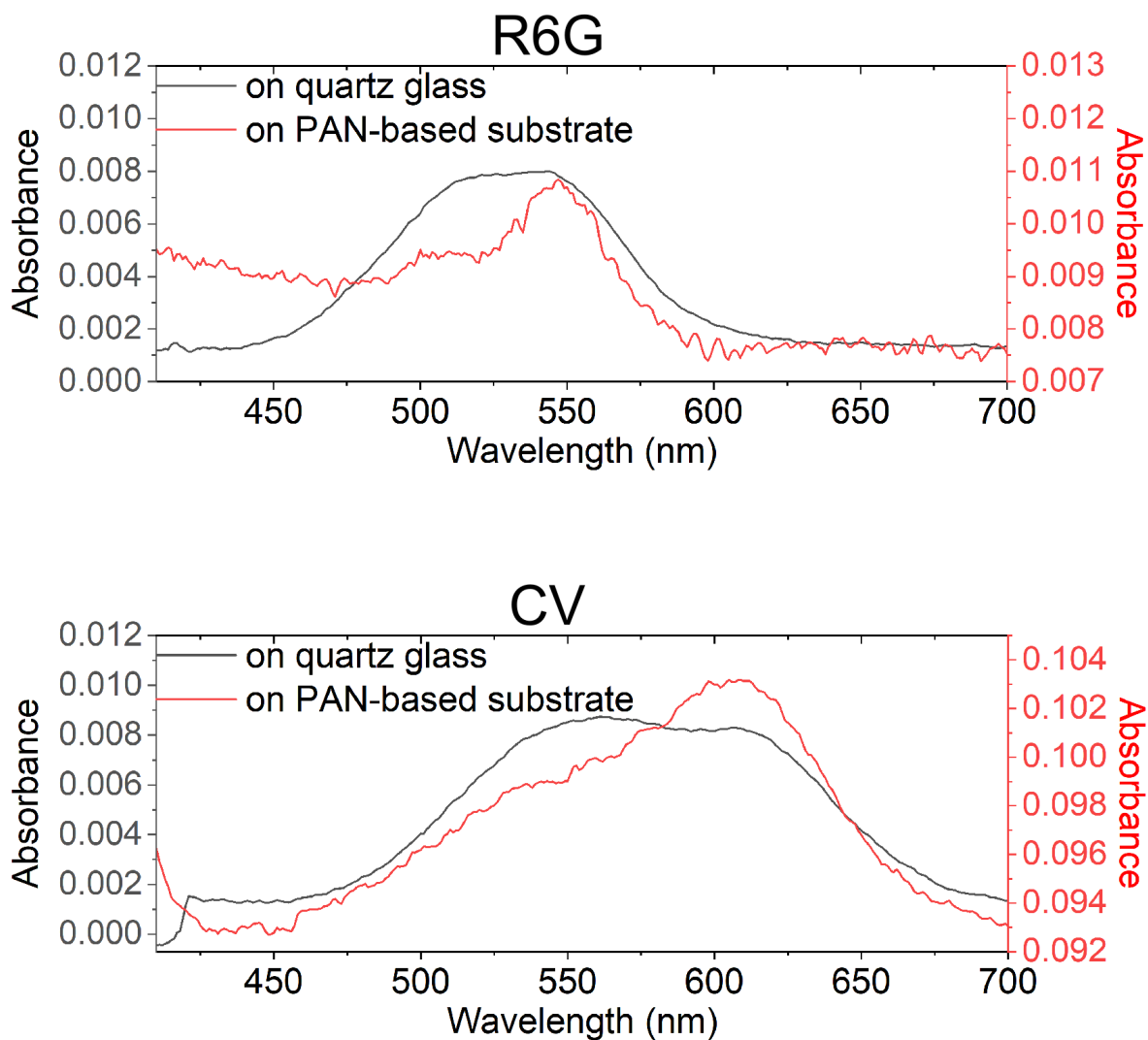| Method	Material	Analyte	EF	LOD	Ref.
Ammo-oxidation	Au nanoparticles/ NH$_3$-Graphene oxide	R6G	5.2×10^4	1 μM	14
Coating	Dimethylformide/Graphene oxide	Rhodamine B	3.2×10^3	10 nM	15
Gas-phase synthesis	N$_2$/Graphite quantum dots	CV	3.2×10^7	100 nM	16
Pyrolysis of N-containing organic materials	Polystyrene-block-poly(x-vinylpyridine) block copolymer, x = 2 or 4	R6G	4.7×10^1	NA	17

Fig. S8 UV-vis absorption spectra of 100 μM R6G and CV on quartz glass and the PAN-based substrate carbonized at 1200 °C.

REFERENCES

1. C. Pardanaud, G. Cartry, L. Lajaunie, R. Arenal and J. G. Buijnsters, *C — J. Carbon Res.,* 2019, **5**, 79.

2. C. Thomsen and S. Reich, *Phys. Rev. Lett.,* 2000, **85**, 5214–5217.

3. M. S. Dresselhaus, G. Dresselhaus and M. Hofmann, *Philos. Trans. A Math. Phys. Eng. Sci.,* 2008, **366**, 231–236.

4. G. Katagiri, *Tanso,* 1996, **1996**, 304–313.

5. N. Melanitis, P. L. Tetlow and C. Galiotis, *J. Mater. Sci.,* 1996, **31**, 851–860.

6. S. Niyogi, E. Bekyarova, M. E. Itkis, H. Zhang, K. Shepperd, J. Hicks, M. Sprinkle, C. Berger, C.

N. Lau, W. A. deHeer, E. H. Conrad and R. C. Haddon, *Nano Lett.*, 2010, **10**, 4061–4066.

7.   T. Takahagi, I. Shimada, M. Fukuhara, K. Morita and A. Ishitani, *J. Polym. Sci. A,* 1986, **24**, 3101–3107.

8.   K. Nukada and K. Kobori, *Kobunshi,* 1974, **23**, 445–448.

9.   R. S. Havigh and H. M. Chenari, *Sci. Rep.,* 2022, **12**, 10704–10717.

10. G. Zhou, S. Yu, L. He, Q. Guo and H. Ye, *Phil. Mag.*, 2012, **92**, 1198–1211.

11. B. Warren, *Phys. Rev.*, 1941, **59**, 693–698.

12. J. Biscoe and B. E. Warren, *J. Appl. Phys.,* 1942, **13**, 364–371.

13. V. Buschmann, B. Kramer, F. Koberling, R. Macdonald and S. Ruttinge, *Application Note. PicoQuant GmbH:* Berlin 2009.

14. M. Kasztelan, A. Słoniewska, M. Gorzkowski, A. Lewera, B. Pałys and S. Zoladek, *Appl. Surf. Sci.*, 2021, **554**, 149060.

15. R. Das, S. Perveen, A. Bora and P. K. Giri, *Carbon*, 2020, **160**, 273–286.

16. M. Keshavarz, A. K. M. R. H. Chowdhury, P. Kassanos, B. Tan and K. Venkatakrishnan, *Sens. Actuators B*, 2020, **323**, 128703.

17. Y.-S. Sun, C.-F. Lin, S.-T. Luo and C.-Y. Su, *ACS. Appl. Mater. Interfaces*, 2017, **9**, 31235–31244.